EUROPEAN ORGANIZATION FOR NUCLEAR RESEARCH

CERN-EP/87-57
16 March 1987

SEARCH FOR $\bar{p}$-NUCLEUS STATES USING THE ($\bar{p}$, p) KNOCK-OUT REACTION AT 600 MeV/c

E. Aslanides
Centre de Physique des Particules de Marseille, Luminy,
13288 Marseille Cedex 09, France

D.M. Drake and J.C. Peng
Los Alamos National Laboratory, Los Alamos, NM 87545, USA

D. Garreta, P. Birien, G. Bruge, H. Catz, A. Chaumeaux, S. Janouin, D. Legrand,
M.-C. Lemaire, B. Mayer, J. Pain and F. Perrot
CEN Saclay, DPhN-ME, 91191 Gif-sur-Yvette Cedex, France

M. Berrada, J.P. Bocquet, E. Monnand, J. Mougey and P. Perrin
CEN Grenoble, DRF, 38402 St Martin d'Hères, France

O. Bing
Centre de Recherches Nucléaires, 67037 Strasbourg Cedex, France

J. Lichtenstadt and A.I. Yavin
Tel Aviv University*), Ramat Aviv, Tel Aviv 69978, Israel

ABSTRACT

The knock-out reaction A($\bar{p}$, p)X has been used to search for narrow $\bar{p}$-nucleus states. The experiment was performed using the 600 MeV/c antiproton beam at LEAR and the high-resolution and large-acceptance magnetic spectrometer SPES II. The A-dependence of the annihilation-induced proton spectra has been studied on ^{2}H, ^{6}Li, ^{12}C, ^{63}Cu, ^{208}Pb and ^{209}Bi. The quasi-free elastic $\bar{p}p$ scattering observed in the lighter targets, and the comparison with the free $\bar{p}p$ scattering, also observed in this experiment, determine an effective proton number N_{eff} for 1s- and 1p-shell protons. No evidence for narrow bound or resonant $\bar{p}$-nucleus states could be found. Upper limits for their production are one order of magnitude lower than certain theoretical predictions, but consistent with the properties of the $\bar{p}$-nucleus interaction, as established from recent elastic and inelastic scattering as well as from studies of antiprotonic atoms.

(Submitted to Nuclear Physics)

*) Supported in part by the Fund for Basic Research of the Israel Academy of Sciences.

1. INTRODUCTION

The search for $\bar{p}$–nuclear states formed by an antiproton and a nucleus, which are different from the well-known antiprotonic atom states bound by the Coulomb interaction, was made possible at the CERN Low-Energy Antiproton Ring (LEAR) with the availability of intense, pure, high-resolution antiproton beams. The favourable conditions for such states to exist are that the $\bar{p}$–nucleus interaction, described by an optical potential $V^{opt}_{\bar{p}\text{–nucl}}$, is sufficiently attractive, and that the absorptive, imaginary part W(r) near the nuclear surface is not too large. Antiproton–nucleus states could then live long enough to be observed, despite the strong annihilation described by W(r). In the pre-LEAR era, antiprotonic atom data were consistent with a variety of potentials having, in general, a strong absorptive part W(r) and a real part V(r) ranging from repulsive to strongly attractive with values of several hundreds of MeV. Among them, those having strongly attractive V(r) and shallow or short ranged W(r) could accommodate many resonant [1] or bound [2–4] $\bar{p}$–nucleus states. Theoretical predictions for the widths of such states range from a few MeV for unbound resonant states, to $\approx$ 100 MeV for bound states. The predicted production cross-sections of such states are of the order of $d^2\sigma/d\Omega dE \approx 0.25$ mb/sr·MeV [3].

The properties of the $\bar{p}$–nucleus interaction as determined by the recent experiments studying the elastic and inelastic scattering of antiprotons on a series of nuclei [5] as well as the energy shifts and widths of antiprotonic atoms [6], are not very encouraging for the existence of $\bar{p}$–nucleus states. For the $\bar{p}$–nucleus potential they indicate that there are rather deep absorptive imaginary parts W(r) and weak real parts V(r) with $V_0 \leq 50$ MeV, and that in particular near the nuclear surface $W(R) \geq 2V(R)$.

On the other hand, it should be remembered that the observation of narrow ($\Gamma \approx 5$ MeV) Σ-hypernuclear states [7] was unexpected on the basis of our present knowledge of the Σ–nucleus interaction. The Σ's should not be stable in a nucleus because of the strong interaction process $\Sigma + N \rightarrow \Lambda + N$. From a theoretical point of view, uncertainties subsist i) in the derivation of $V^{opt}_{\bar{p}\text{–nucl}}$ from the elementary $\bar{N}N$ potential using folding procedures over the nuclear densities; ii) in the calculation of the $\bar{p}$–nucleus eigenstates E_n–i$\Gamma_n/2$ when solving the Schrödinger equation for deep-lying states only, and neglecting higher-lying states, which require a relativistic treatment; and iii) in the calculations of the production cross-section of the $\bar{p}$–nucleus states through the A($\bar{p}$, p)X reaction, where often only the PWIA is used.

The uncertainties in the presently available theoretical predictions left much room for an experimental search for $\bar{p}$–nucleus states. Such states are easier to identify if they are narrow ($\Gamma \lesssim$ 10 MeV), although experiments with particularly large momentum acceptance and moderate energy resolution looked for broader states, but without success [8].

A first exploratory experiment [9] using about 10^9 antiprotons was devoted to the search for $\bar{p}$–nucleus states through the ($\bar{p}$, p) reaction on scintillator, ^{12}C, ^{63}Cu, and ^{209}Bi targets. In a subsequent experiment [10], ^{6}Li, ^{12}C, scintillator, CD_2, and ^{208}Pb were studied, and high-statistics data could be obtained on the lighter targets. The results of this experiment are reported here together with an analysis of the target mass dependence of the annihilation-induced proton spectra and the quasi-free $\bar{p}p$ scattering cross-sections on individual protons of the ^{2}H, ^{6}Li, and ^{12}C nuclei.

2. EXPERIMENTAL METHOD

The knock-out reaction A($\bar{p}$, p)X has been used to search for $\bar{p}$–nucleus states $\{\bar{p}\text{–}(A-1, Z-1)\}$. These should be identified as discrete energy lines superimposed on the continuous proton spectrum arising from the annihilation of the antiprotons and the subsequent proton knock-out by the annihilation pions. There are two main advantages in using the ($\bar{p}$, p) knock-out reaction: i) the outgoing proton, at $\theta_{lab} = 0°$, carries most of the incoming antiproton momentum, leaving the antiproton almost 'recoilless' in the target, thus favouring the formation of $\bar{p}$–nucleus states; ii) one

can choose the momentum of the incident antiproton close to the maximum (at $p_{\bar{p}} \approx 500$ MeV/c) of the backward $\bar{p}p$ scattering cross-section [11] in order to improve the yield of the A($\bar{p}$, p)X reaction.

For the present studies the 600 MeV/c LEAR beam was used with an average intensity of $\approx 10^5$ antiprotons per second during the 60 min. long beam spills. The beam intensity was measured with a 360 μm thick scintillator located 25 cm upstream of the target.

The outgoing protons were detected at $\theta_{lab} = 0°$ and momentum-analysed with the magnetic spectrometer SPES II (see fig. 1), which has a momentum acceptance $\Delta p/p = \pm 18\%$, a solid angle $\Delta\Omega = 30$ msr, and a momentum resolution of 5×10^{-4}. Protons were unambiguously identified by time-of-flight, which eliminated pions due to annihilations in the target [12]. In tuning the magnetic field for the detection of positive particles at 0°, the incoming antiproton beam, which did not interact in the target, could also enter the spectrometer and stop inside the vacuum chamber of the first dipole magnet. A 2 cm thick scintillator S_5 was positioned inside this dipole on the beam trajectories and was used to efficiently veto charged-particle background (essentially π^+) due to this beam annihilation.

The total number of antiprotons used on the different targets were 2.5×10^9 $\bar{p}$ on ^{6}Li (1.92 g/cm^2), 5.0×10^9 $\bar{p}$ on C (0.76 g/cm^2), 6.8×10^9 $\bar{p}$ on scintillator (2.10 g/cm^2), 6.8×10^9 $\bar{p}$ on CD_2 (1.03 g/cm^2), and 2.7×10^8 $\bar{p}$ on ^{208}Pb (1.97 g/cm^2). The overall proton detection efficiency varied between 96% and 99%. The energy resolution of the outgoing protons was about 1.5 MeV, essentially due to the energy-loss straggling in the targets and to the multiple scattering effects in the target, in the spectrometer windows and in the detection system.

The estimated beam loss by annihilation in the targets was small — 1.1% to 2.5% depending on the target thickness and mass A. The absolute normalization uncertainties on the measured cross-sections are $\lesssim 10\%$.

3. RESULTS AND DISCUSSION

Proton energy spectra observed with the various targets are shown in figs. 2 to 6, where the double differential cross-sections $d^2\sigma/d\Omega dE$ are plotted as a function of the outgoing proton energy. The different signs for the experimental points correspond to different magnetic field settings of the spectrometer. The upper scale represents the mass difference M(X) − M(A). The proton energy range and the corresponding binding energy difference $B_p - B_{\bar{p}}$ of the proton or the antiproton in the core nucleus (A − 1, Z − 1) are given for convenience in table 1.

As expected, the proton spectra are dominated by protons produced by the antiproton annihilation in the target nucleus and the subsequent proton ejection by the produced pions, either directly or indirectly through Δ-isobar formation. In the following we discuss i) these continuous spectra and their dependence on the nuclear mass A, which is interesting since they are the main physical background in the search for $\bar{p}$–nucleus states; ii) the observation of the quasi-free backward elastic scattering on individual protons of the target nucleus; and iii) the absence of any narrow ($\approx$ a few MeV) structure due to bound or resonant $\bar{p}$–nucleus states and the upper limits put by the present work on the production cross-sections for such states.

3.1 Inclusive proton cross-sections and their A-dependence

The inclusive secondary proton spectra can be described by a Maxwellian distribution $d^2\sigma/d\Omega dE = C\sqrt{E}\exp(-E/T)$, where T is regarded as an effective temperature. Table 2 gives the temperatures obtained for the different targets in fitting the above expression to the data. A general trend in the results is that the effective temperature decreases with the target mass.

Energy spectra of protons emitted after antiproton annihilation in nuclei have been calculated by different groups [13, 14] in the framework of the intranuclear cascade (INC) model. It is based on the simple physical picture of the antiproton annihilating on a single nucleon, generating a number of

pions, which then cascade through the nucleus interacting with the remaining nucleons. Although such calculations are meaningful only for heavier nuclei, the result of a calculation for the $\bar{p}$ + ^{12}C annihilation proton spectra at 600 MeV/c [14] is shown in figs. 3 and 5 as a dashed line. The predicted slope, T = 62 MeV, is steeper than in the measured spectra from which an effective temperature of 86 MeV (full line) can be deduced.

This simple INC model describes well the overall gross features of the experimental data on the antiproton annihilation in nuclei [8, 15]. The quantitative understanding of these data necessitates refined INC calculations, taking into account the location of the annihilation inside or at the surface of the nucleus, the energy of the pions, and the attenuation of both the pions and the ejected protons as a function of their energy or the use of a more realistic picture of the $\bar{p}$-nucleus annihilation.

The dependence of the proton production cross-section in the continuum on the target mass A was determined on the heavier targets C, Cu, and Bi to be $\propto A^{2/3}$ [9]. Such a nuclear mass dependence is to be expected for a hadronic strong interaction process such as the antiproton annihilation. The INC calculations, also predicted a similar A-dependence. The measurements of ^{6}Li (fig. 2) and D, deduced from the CD_2 measurements after the subtraction of the carbon contribution (fig. 6), exhibit a stronger dependence, about $\propto A^{1.7}$. This is shown in fig. 7, which displays, for convenience, the ratio of the double differential cross-sections at $\theta_{lab} = 0°$ and $E_p = E_{\bar{p}}$ on the various targets to the carbon cross-section as a function of the corresponding mass ratio $A_i/12$ (dark points). The $A^{2/3}$-dependence is drawn as a full line for the heavier targets ($A \geq 12$), and the $A^{1.7}$-dependence as a dashed line for the lighter targets ($A \leq 12$). Such a mass dependence can be understood if one considers the two main processes contributing to the proton production: i) the antiproton annihilation in the nucleus, with the well-established $A^{2/3}$-dependence, giving rise to an average number of five pions, and ii) the ejection of a proton from among those remaining after the annihilation (if one neglects to first order the $\pi^+ n \rightarrow \pi^0 p$ charge-exchange contribution of $\approx 20\%$).

Light targets are rather transparent to the pions, and process (ii) should depend directly on the number of the available protons after annihilation. On the average this number is [Z − (Z/A)], and for Z = N nuclei (Z − $^1/_2$). This leads to an overall (A, Z)-dependence of $\approx A^{2/3}(Z - {}^1/_2)$ or $\approx A^{2/3}(A - 1)$.

In heavier targets the probability for pions to interact is saturated—the nuclei are 'opaque' to the pions and thus no additional mass dependence is to be added to the $A^{2/3}$-dependence of the annihilation.

The above proposed physical picture should be replaced by more elaborate calculations taking into account all processes contributing to the proton ejection by the annihilation pions and resulting in a mass dependence with a smooth transition between the two regimes.

The fourth column in Table 2 gives the energy integrated cross-sections $d\sigma/d\Omega$ at $\theta_{lab} = 0°$. As can be seen on fig. 7 (open circles) the dependence of these cross-sections on the target mass, A, is nearly the same as observed for the double differential cross-sections. This is not surprising in view of the small differences in the effective temperatures of the different targets.

The integration of the differential cross-sections over the solid angle required the knowledge of the angular distributions of the proton spectra. In our previous work [9] the proton energy spectra on ^{12}C had also been measured at 40°. Angular distributions for the energy integrated proton cross-sections have also been calculated for ^{12}C and ^{238}U [14] and for ^{40}Ca and ^{108}Ag [13] in the INC framework. The angular distributions from ref. [14] and our previous work [9] are similar.

The total proton production cross-section we obtain for ^{12}C using the angular distribution of ref. [14] is $\sigma^p_{tot} = 520 \pm 30$ mb. Using the angular distribution of the same reference for ^{238}U, the total proton cross-sections for ^{208}Pb and ^{209}Bi would be 3520 ± 690 mb and 4110 ± 660 mb respectively.

Comparing these integrated proton cross-sections to the reaction cross-section σ_R on the same nuclei [5] leads to an average number of protons produced per annihilation which is 1.04 ± 0.06 for ^{12}C, 1.3 ± 0.3 for ^{208}Pb and 1.5 ± 0.3 for ^{209}Bi.

3.2 Quasi-free scattering and effective proton number

The backward (180°) elastic scattering $\bar{p}p \rightarrow p\bar{p}$ of the antiprotons on hydrogen was easily identified as a narrow proton line at $E_p = E_{\bar{p}}$ in the proton spectra measured with the scintillator target (see fig. 5). The average value of all our measurements (including those reported ealier [9]) of the c.m. differential cross-section for this reaction is $d\sigma/d\Omega^*$ (180°) = 0.66 ± 0.03 mb/sr, to be compared with the value of 0.65 ± 0.05 mb/sr that can be deduced from an earlier [11] excitation study.

The prominent structure in the CD_2 spectrum (fig. 6a) is due to the quasi-free backward $\bar{p}p$ scattering on the proton in deuterium. Figure 6b shows the proton spectrum after subtraction of the carbon continuum. The differential cross-section for this reaction is $d\sigma/d\Omega$ = (1437 ± 41) μb/sr (see table 3).

The quasi-free $\bar{p}p$ scattering was difficult to observe in the heavier targets, despite its relatively large cross-section, because of the proton continuum background, which has the strong A-dependence discussed in the previous section. Narrow structures to be attributed to this process could be observed with the ^6Li target (fig. 2) and with larger systematic uncertainties on ^{12}C in a high-statistics measurement using the scintillator target (fig. 8a, b).

Calculations of the quasi-free scattering have been carried out for ^2H, ^6Li and ^{12}C, using a simple picture in which the recoil (A − 1, Z − 1) nucleus and the hit proton move back-to-back with the proton's internal momentum before the collision.

For deuterium a McGee type parametrization [16] of the Reid soft-core wave function has been used. Internal momentum distributions of the form $F(k) \sim \sin^2(\pi k/k_{F_{max}})$ were assumed for the 1p-shell protons in ^6Li and ^{12}C. For the Fermi momenta $k_{F_{max}}$, those determined from quasi-free electron scattering on nuclei [17] were adopted. The results are represented in figs. 2, 6 and 8. The calculated spectra have been scaled down in intensity by the ratio of the corresponding differential cross-section to the free $\bar{p}p \rightarrow p\bar{p}$ cross-section, which can be regarded as an effective number N_{eff} of protons in the target nucleus.

In the ^6Li case, the calculation of the quasi-free scattering on 1p-shell protons (dash-dotted line in fig. 2) is in good agreement with the observed bumps near 168 MeV and confirms the quasi-free peak interpretation. The lower-energy shoulder near 155 MeV could be due to the antiproton scattering on 1s-shell protons, which would give rise to a bump around 154 MeV, as represented by the dotted line in fig. 2.

In the carbon case the determination of the quasi-free peak position and intensity has large uncertainties due to the statistics and mainly to the subtraction of the continuum contribution. The calculated quasi-free proton bump position due to antiproton scattering on 1p-shell protons is ≈ 6 MeV lower than experimentally observed (see fig. 8b). The discrepancy may be explained by the Coulomb corrections not included in the calculations and which are small in the case of ^6Li. For the sake of completeness, as in the ^6Li case, the quasi-free contribution from the 1s-shell protons in ^{12}C is shown as a dotted line in fig. 8b. The overall shape is in good agreement with the experimental one but, given the present experimental inaccuracies, no meaningful discussion of the shape and its position could be made.

Table 3 summarizes the differential cross-sections for the quasi-free scattering, the corresponding statistical and systematic errors, and the effective proton numbers corresponding to the various targets, defined as $N_{eff} = d\sigma[\bar{p}A \rightarrow p(A-1)\bar{p}]/d\sigma(\bar{p}p \rightarrow p\bar{p})$. The effective proton

numbers determined for ^{6}Li and ^{12}C are smaller than the theoretical estimate of $N_{eff} = 0.5$ [18]. They are also smaller than the number $\sigma(\bar{p}C \rightarrow \bar{n}X)/\sigma(\bar{p}p \rightarrow \bar{n}n) = 0.86 \pm 0.05$ reported for the charge-exchange reactions on carbon and hydrogen [19].

Part of the discrepancy between the two experimentally determined effective proton numbers could be due to the large difference in the momentum acceptance and in the energy and angular resolutions.

The explanation of the observed difference may also be related to the nature of the underlying 'elementary' processes: the charge exchange $\bar{p}p \rightarrow \bar{n}n$ for the $A(\bar{p}, \bar{n})X$ reaction, and the antiproton backward scattering (or protron knock-out) $\bar{p}p \rightarrow p\bar{p}$ for the $A(\bar{p}, p)_{quasi\text{-}free}$ reaction. The former proceeds through one-pion exchange, implying a long-range (λ_1) interaction of the incoming antiprotons, which can, therefore, interact with the target nucleus without entering the nucleus. The latter proceeds through ϱ, ω, or heavier meson-exchange, implying a short-range (λ_2) interaction of the incoming $\bar{p}$ and consequently a large annihilation probability. The ratio r of the total probabilities for these two types of processes on a given nucleus of radius R can be roughly estimated by the geometrical expression $r = [(R + \lambda_1)^2 - R^2]/[(R + \lambda_2)^2 - R^2]$, where the interaction cross-section is $\approx (R + \lambda_i)^2$, and the antiproton flux attenuation due to the annihilation is $\approx R^2$. Taking currently accepted values $\lambda_1 = 1.5$ fm, $\lambda_2 = 0.5$ fm, and $R \simeq 1.2\, A^{1/3}$ fm, we find for carbon, $r_{^{12}C} \simeq 3.5$. Such a reduction factor is not very different from the experimental ratio $N_{eff}(\bar{p}, \bar{n})/N_{eff}(\bar{p}, p)_{quasi\text{-}free}$ of the effective proton numbers measured through the $(\bar{p}, \bar{n})$ and the quasi-free $(\bar{p}, p)$ reactions, respectively.

3.3 Upper limits for the production of narrow $\bar{p}$–nucleus states

With the exception of the quasi-free scattering peaks, no narrow proton lines could be found in the proton spectra produced on the various targets. The use of a CD_2 target was useful in measuring the quasi-free $(\bar{p}, p)$ cross-section and in estimating the annihilation continuum background on deuterium. This target was not appropriate for the search for $\{\bar{p}\text{–}n\}$ states, nor was it competitive with a cryogenic target.

Experimental upper limits for the production cross-section of narrow antiprotonic states can be deduced, in Li, C, and Pb, for different outgoing proton energies and level widths. The values (3σ) quoted in table 4 have been estimated considering proton energies close to the incident antiproton energy, i.e. states in which the antiproton binding energy is close to the binding energy of the ejected proton. A level width of 2 MeV has been assumed. The upper limits deduced from the most statistically significant measurements, those on Li and C, are more than one order of magnitude lower than theoretically predicted for the production of such $\bar{p}$–nucleus states.

Direct comparisons of the experimental results with the existing theoretical predictions is difficult because of the antiproton energies and nuclear targets considered. However, some comments can be made regarding the comparison with the work of Gibbs and Kaufmann [20] and with that of Heiselberg et al. [3].

Although not directly related to the physics of the present paper, the production of low-lying antiprotonic atom levels through the $(\bar{p}, p)$ reaction is interesting because such levels should have shifts and widths larger than those observed in usual antiproton-cascade X-ray measurements. The production cross-sections are predicted to be a few μb/sr* at 0°. The relatively strong antiproton binding would be, for example for $^{18}O_{2S}$, about 0.5 MeV, but the widths of these Coulomb states should be small, $\Gamma_{^{18}O_{2S}} \simeq 34$ keV. Scaling the results of ref. [19], at $E_{\bar{p}} = 100$ MeV, up to $E_{\bar{p}} = 180$ MeV, the differential cross-section for the $^{19}F(\bar{p}, p)\{\bar{p}\text{–}^{18}O\}_{2S}$ reaction would be $d\sigma/d\Omega\,(0°) \simeq 4.9$ μb/sr. Given the energy resolution of our apparatus, ≈ 1.5 MeV, the double differential cross-section at the peak amplitude for this state would be 0.17 μb/sr · MeV. If we use the carbon data and the $A^{2/3}$-dependence for the proton continuum background, the double differential

cross-sections for the background expected with a ^{19}F target would be about 220 μb/sr·MeV. The detection of the above atomic states, corresponding to proton energies slightly ($\approx$ 7.5 MeV) below the incident antiproton beam energy, was obviously out of reach of the present experiment.

The predictions of Heiselberg et al. [3] for the production of bound states were made for the $^{16}O(\bar{p}, p)$ reaction at $E_{\bar{p}} \simeq 20$ to 100 MeV, using optical potential parameters determined before the recent studies of the $\bar{p}$-nucleus interaction at LEAR [5, 6]. For a qualitative comparison with the experiment, their predictions can be scaled up in energy to $E_{\bar{p}} = 180$ MeV and down in the real part, $V_0 \simeq 300$ MeV, of the optical potential to $V_0 \simeq 50$ MeV. The result would be a bump in the proton energy spectrum at $E_p \simeq 270$ MeV with an amplitude cross-section of 0.28 mb/sr·MeV and a width of 160 MeV.

The highest proton energy values measured in our experiments are $E_p \simeq 290$ MeV. Within this limitation the following remarks can be made on the high-statistics measurements on carbon. The differential cross-sections are exponentially decreasing from $\approx$ 230 μb/sr·MeV at 120 MeV to $\approx$ 50 μb/sr·MeV at 290 MeV. No deviation from this exponential fall-off has been noticed and, more specifically, the cross-section at the suggested proton energy peak at 270 MeV is much lower than the expected value of 0.28 mb/sr·MeV.

4. SUMMARY AND CONCLUSION

The study of the proton spectra produced on various targets through the $(\bar{p}, p)$ knock-out reaction at 600 MeV/c allowed a quantitative understanding of the annihilation-induced proton continuum and its dependence on the target mass.

The quasi-free scattering cross-sections could be observed on the individual protons of the lighter targets, for which an effective number of protons could be defined by comparison with the free $\bar{p}p \rightarrow p\bar{p}$ cross-section at the same energy.

The present study showed no evidence for the existence of narrow bound or resonant $\bar{p}$-nucleus states. The upper limits set on the production cross-section of such states are about one order of magnitude lower than the various theoretical predictions. However, the present experimental results are consistent with the nature of the $\bar{p}$-nucleus interaction as established by the recent high-quality elastic and inelastic scattering as well as by the antiprotonic atom data.

Recently [21] the strong spin and/or isospin dependence of the imaginary part of the $\bar{N}N$ interaction was considered for a possible reduction of the annihilation probability of antiprotons in nuclei. This led to the hypothesis that the $\bar{N}NN$ or $\bar{N}NNN$ systems might form relatively narrow bound states. Practically, the reaction $\bar{p} + {}^3He \rightarrow p + X$ with $X \equiv \{\bar{p}\text{–}(pn)\}$ can be considered.

Future generation experiments searching for antiprotonic bound or resonant states will require high resolution and large acceptance detectors, similar to the present one, but will also aim at considerably higher statistics $\geq 10^{11}$ $\bar{p}$. In order to initiate such an experimental program more theoretical calculations would be needed, taking into account the now established properties of the $\bar{p}$-nucleus interaction as well as the nuclear structure of the involved specific nuclear states.

Acknowledgements

We are grateful to the LEAR staff and the South Hall team, whose competence and assistance made these experiments possible during the early LEAR operation. Thanks are due to E. Klempt, A. Bouyssy and J.M. Richard for helpful discussions and suggestions.

REFERENCES

[1] E.H. Auerbach, C.B. Dover and S.H. Kahana, Phys. Rev. Lett. **46** (1981) 702.

[2] A.M. Green and S. Wyceh, Nucl. Phys. **A377** (1982) 441.

[3] H. Heiselberg et al., Phys. Lett. **132B** (1983) 279.

[4] C.Y. Wong et al., Phys. Rev. **C29** (1984) 574.

[5] D. Garreta et al., Proc. 3rd LEAR Workshop on Physics with Antiprotons at LEAR in the ACOL Era, Tignes, 1985 (Éditions Frontières, Gif-sur-Yvette, 1985), p. 599.

[6] H. Poth et al., ibid., p. 581.

[7] See, for example, Proc. Int. Conf. on Hypernuclear and Kaon Physics, Heidelberg, 1982 (Max-Planck Inst., Heidelberg, 1982).

[8] J.W. Sunier et al., Proc. VII^{e} European Symposium on Antiproton Interactions, Durham, United Kingdom, 1984 (A. Hilger, Bristol, 1985), p. 195.
P.L. McGaughey et al., Phys. Rev. Lett. **56** (1986) 2156.

[9] D. Garreta et al., Phys. Lett. **150B** (1985) 95.

[10] E. Aslanides et al., Proc. 3rd LEAR Workshop, Tignes, 1985, p. 615.

[11] M. Alston-Garnjost et al., Phys. Rev. Lett. **43** (1979) 1901.

[12] D. Garreta et al., Phys. Lett. **135B** (1984) 266.

[13] M. Cahay et al., Phys. Lett. **B115** (1982) 7.
M. Cahay, J. Cugnon and J. Vandermeulen, Nucl. Phys. **A393** (1983) 237.

[14] M.R. Clover et al., Phys. Rev. **C26** (1982) 2138.

[15] G. Piragino et al., Proc. 3rd LEAR Workshop, Tignes, 1985, p. 621.

[16] J.M. Laget, Nucl. Phys. **A296** (1978) 388.
P. Bosted and J.M. Laget, Nucl. Phys. **A296** (1978) 413.

[17] E.J. Moniz et al., Phys. Rev. Lett. **26** (1971) 445.

[18] A. Bouyssy, private communication.

[19] K. Nakamura et al., Phys. Rev. **C31** (1985) 1853.

[20] W.R. Gibbs and W.B. Kaufmann, Phys. Lett. **145B** (1984) 1.

[21] A.J. Baltz et al., Phys. Rev. **C32** (1985) 1272.

Table 1

Proton energy range E_p measured for the various targets and the corresponding range of binding energy difference, $B_p - B_{\bar{p}}$, of the proton or the antiproton in the core $(A-1, Z-1)$.

Target	$E_{\bar{p}}$ (MeV)	E_p range (MeV)	$B_p - B_{\bar{p}}$ (MeV)
^{6}Li	177.9	134 - 294	44 - (−116)
^{12}C	179.7	106 - 210	74 - (−30)
^{208}Pb	179.2	139 - 229	62 - (−50)
Scint.	176.5	117 - 291	60 - (−114)
CD_2	178.8	106 - 210	73 - (−31)

Table 2

Temperatures T obtained from the best fit of the Maxwellian expression $C\sqrt{E}\exp(-E/T)$ to the proton energy spectra and the energy integrated differential cross-sections at $\theta_{lab} = 0°$.

Target	T (MeV)	C (μb/sr MeV$^{3/2}$)	$d\sigma/d\Omega$ (0°) (mb/sr)	
^{6}Li	101 ± 4	17.3	15.6 ± 0.9	
^{12}C [a)]	86 ± 1.5	84	59.4 ± 1.6	Ref. [9] and present work
^{63}Cu	69 ± 10	405	206 ± 45	Ref. [9]
^{208}Pb	72 ± 9	619	335 ± 63	
^{209}Bi	69 ± 7	770	391 ± 60	Ref. [9]

a) Also taken into account are the measurements on the scintillator target whose continuum is exclusively due to the carbon component.

Table 3

Quasi-free backward elastic $\bar{p}p$ scattering cross-sections:
δ_{stat} are the statistical errors and δ_{syst} the systematic uncertainties
due mainly to the continuum subtraction; N_{eff} is the effective proton number.

Target	$d\sigma/d\Omega$ (180°) (μb/sr)	δ_{stat} (μb/sr)	δ_{syst} (μb/sr)	N_{eff}	Proton shell
^{2}H	1437	±41	±46	0.53 ± 0.06	1s
^{6}Li	386	±16	±40	0.15 ± 0.03	1p
	216	±16	±40	0.09 ± 0.03	1s
^{12}C	304	±30	±112	0.11 ± 0.06	1p
	135	±23	±80	0.05 ± 0.04	1s

Table 4

Upper limits (3σ) for the production cross-section of
$\bar{p}$–nucleus states through the ($\bar{p}$, p) reaction,
assuming a level width of 2 MeV and an antiproton
binding energy equal to the initial protons.

Target	$\bar{p}$–nucleus state	$(d\sigma/d\Omega)_{U.L.}$ (μb/sr)
^{6}Li	$\{\bar{p}$–$^{5}He\}$	12
^{12}C	$\{\bar{p}$–$^{11}B\}$	18
^{208}Pb	$\{\bar{p}$–$^{207}Tl\}$	630

Figure captions

Fig. 1: a) Schematic layout of the SPES II magnetic spectrometer facility. Particles travel in vacuum from the quadrupole entrance to the first localization MWPC, inside a vacuum chamber not shown in this figure.

b) Details of the antiproton beam-pipe end and the target region.

Fig. 2: Double differential cross-sections for the $^{6}Li(\bar{p}, p)X$ reaction at $E_{\bar{p}} = 177.9$ MeV. The full line corresponds to an average temperature T = 101 MeV. The dash-dotted line is the result of a quasi-free scattering calculation corresponding to an effective proton number N_{eff} = 0.15. The dotted line represents the contribution of the quasi-free scattering on 1s-shell protons with an effective proton number 0.09.

Fig. 3: Double differential cross-sections for the $^{12}C(\bar{p}, p)X$ reaction at $E_{\bar{p}} = 179.7$ MeV. The full line corresponds to an average temperature T = 86 MeV. The dashed line is the result of the INC calculation with T = 62 MeV.

Fig. 4: Double differential cross-sections for the $^{208}Pb(\bar{p}, p)X$ reaction at $E_{\bar{p}} = 179.2$ MeV. The full line corresponds to an average temperature T = 72 MeV.

Fig. 5: Double differential cross-sections for the $(\bar{p}, p)X$ reaction on a scintillator target at $E_{\bar{p}}$ = 176.5 MeV. The sharp peak at M(X) = M(A) corresponds to the backward elastic $\bar{p}p$ scattering on hydrogen. The full line corresponds to an average temperature T = 86 MeV, and the dashed line represents an INC calculation with T = 62 MeV.

Fig. 6: a) Double differential cross-sections for the $(\bar{p}, p)X$ reaction on a CD_2 target at $E_{\bar{p}} = 178.8$ MeV. The full line represents the best fit to the proton spectra produced on carbon. The dotted line represents the quasi-free scattering calculation on deuterium with N_{eff} = 0.53, superimposed to the carbon continuum.

b) Double differential cross-sections for the $D(\bar{p}, p)X$ reaction obtained from the CD_2 spectra after subtraction of the carbon contribution (best fit). The dotted line represents the same quasi-free scattering result as in part a).

Fig. 7: Dependence of the differential cross-section for proton production in the continuum as a function of the target mass A. The full line corresponds to a mass dependence $\propto A^{2/3}$ and the dashed line to a mass dependence $\propto A^{1.7}$.

Fig. 8: a) Proton spectrum produced on the scintillator target. The full line is the best fit of the carbon continuum. The dash-dotted curve represents the quasi-free scattering calculation on 1p-shell protons with $N_{eff} = 0.11$.

b) The proton spectrum after subtraction of the annihilation continuum. The dash-dotted line represents the quasi-free scattering calculation on 1p-shell protons with N_{eff} = 0.11. The dotted line shows the contribution of the quasi-free scattering on 1s-shell protons with N_{eff} = 0.05.

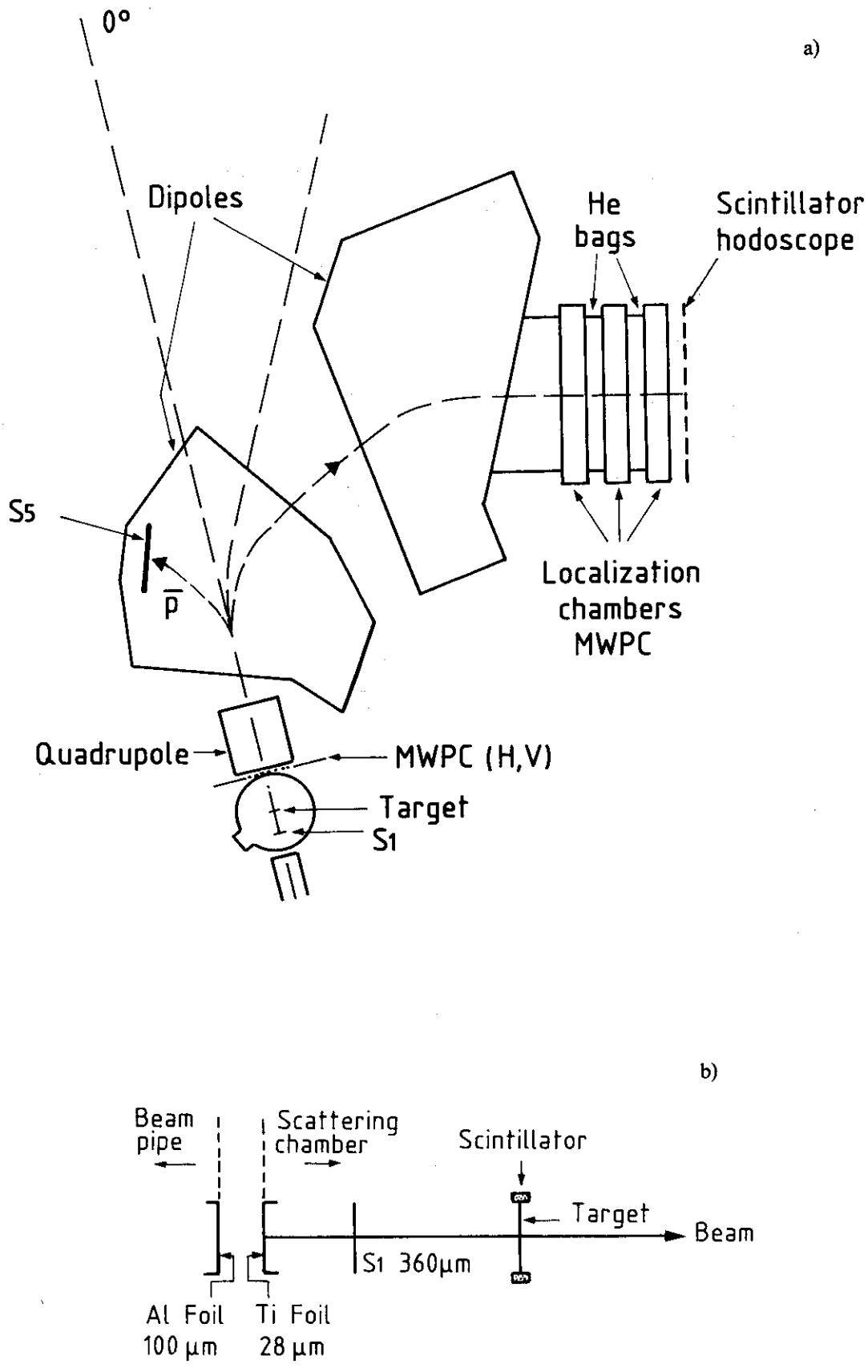
a)
0°
Dipoles
He
bags
Scintillator
hodoscope
S5
$\bar{p}$
Localization
chambers
MWPC
Quadrupole
MWPC (H,V)
Target
S1
b)
Beam
pipe
Scattering
chamber
Scintillator
Target
Beam
S1 360µm
Al Foil
100 µm
Ti Foil
28 µm

Fig. 1

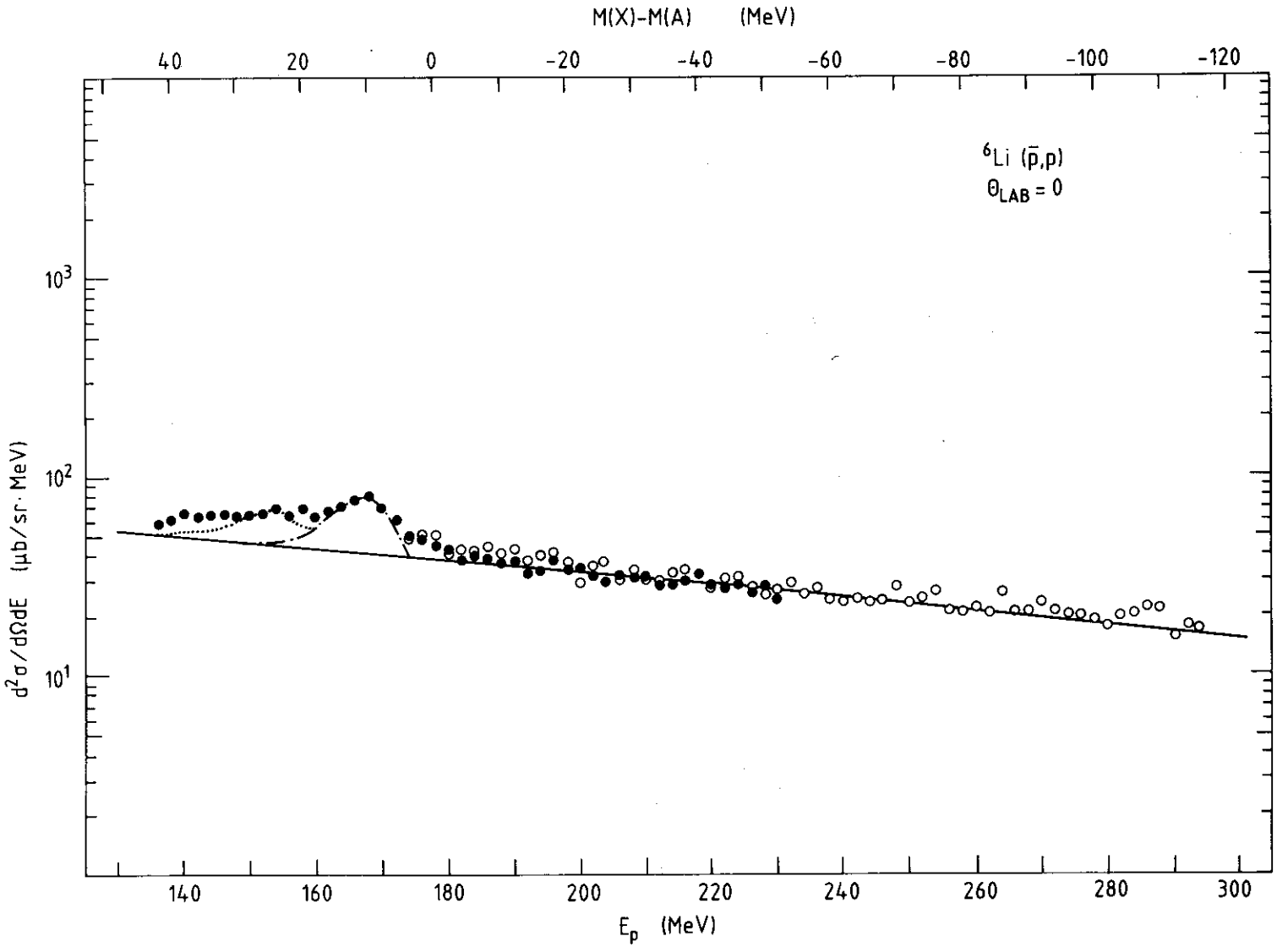
M(X)-M(A) (MeV)
40
20
0
-20
-40
-60
-80
-100
-120
^{6}Li ($\bar{p}$,p)
Θ_{LAB} = 0
10^3
10^2
10^1
$d^2\sigma/d\Omega dE$ (μb/sr·MeV)
140
160
180
200
220
240
260
280
300
E_p (MeV)

Fig. 2

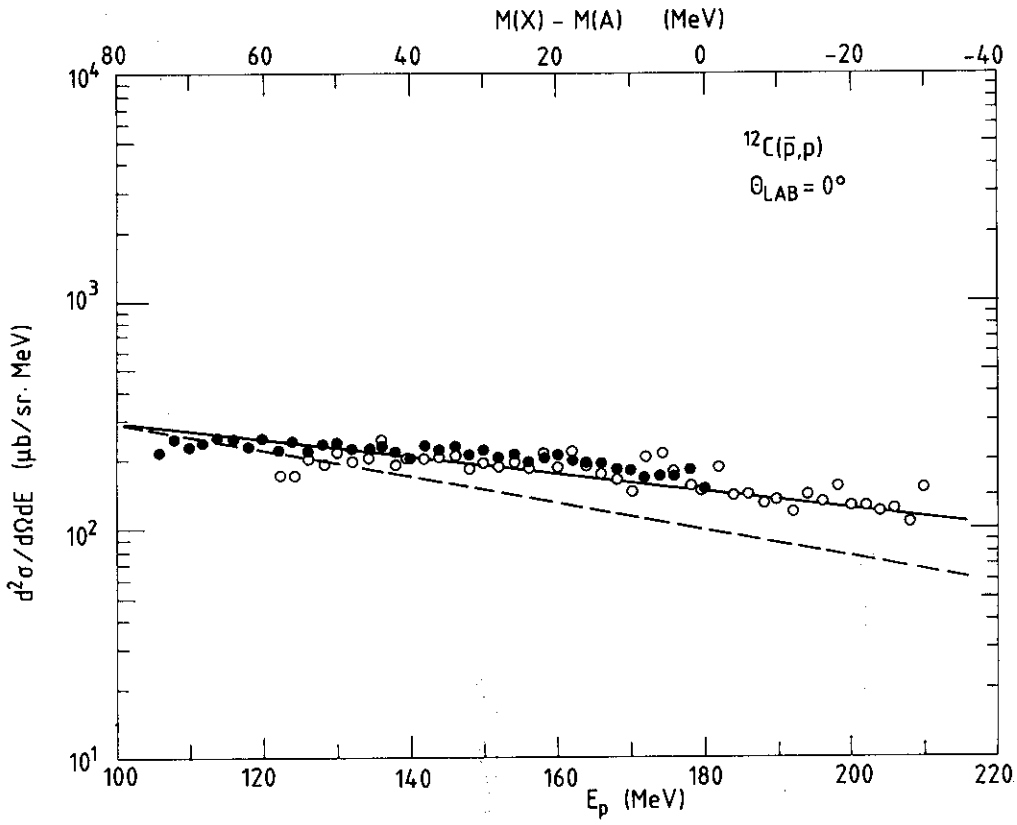
M(X) - M(A) (MeV)
80
60
40
20
0
-20
-40
10^4
10^3
10^2
10^1
$^{12}C(\bar{p},p)$
$\Theta_{LAB} = 0°$
$d^2\sigma/d\Omega dE$ (μb/sr. MeV)
100
120
140
160
180
200
220
E_p (MeV)

Fig. 3

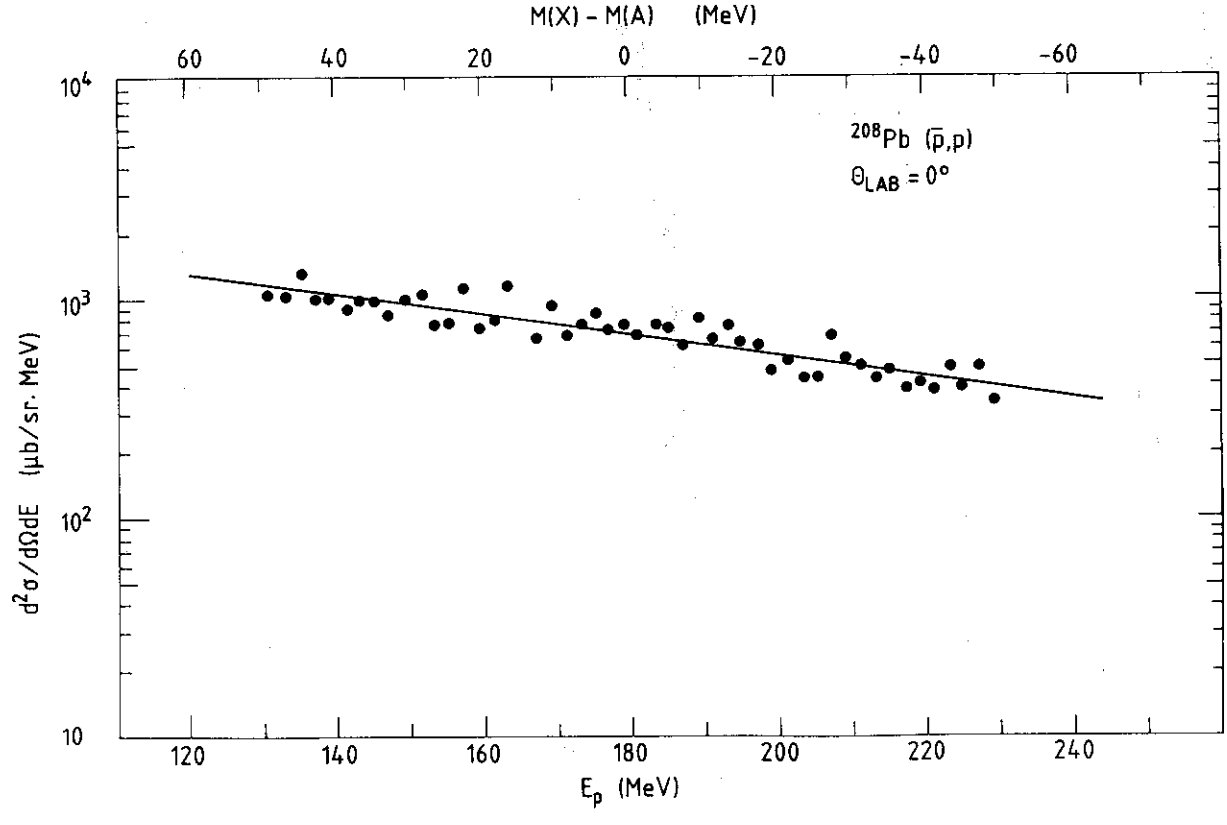
M(X) - M(A) (MeV)
60
40
20
0
-20
-40
-60
10^4
10^3
10^2
10
^{208}Pb $(\bar{p},p)$
$\Theta_{LAB} = 0°$
$d^2\sigma/d\Omega dE$ (μb/sr. MeV)
120
140
160
180
200
220
240
E_p (MeV)

Fig. 4

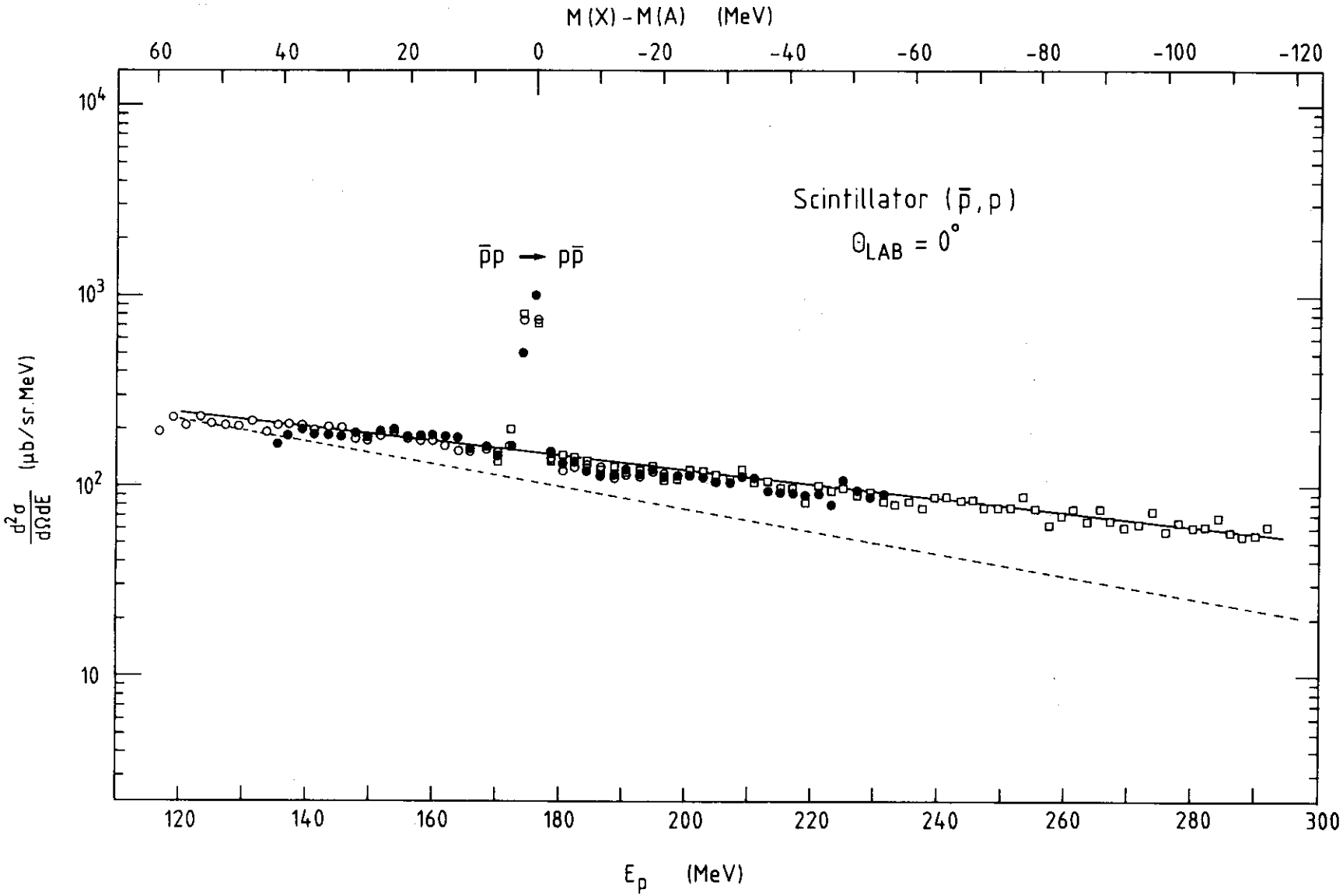
M(X) - M(A) (MeV)
60
40
20
0
-20
-40
-60
-80
-100
-120
10^4
10^3
10^2
10
$\frac{d^2\sigma}{d\Omega dE}$ (μb/sr.MeV)
Scintillator (p̄, p)
$\Theta_{LAB} = 0^\circ$
p̄p → pp̄
Θ_{CM}
120
140
160
180
200
220
240
260
280
300
E_p (MeV)

Fig. 5

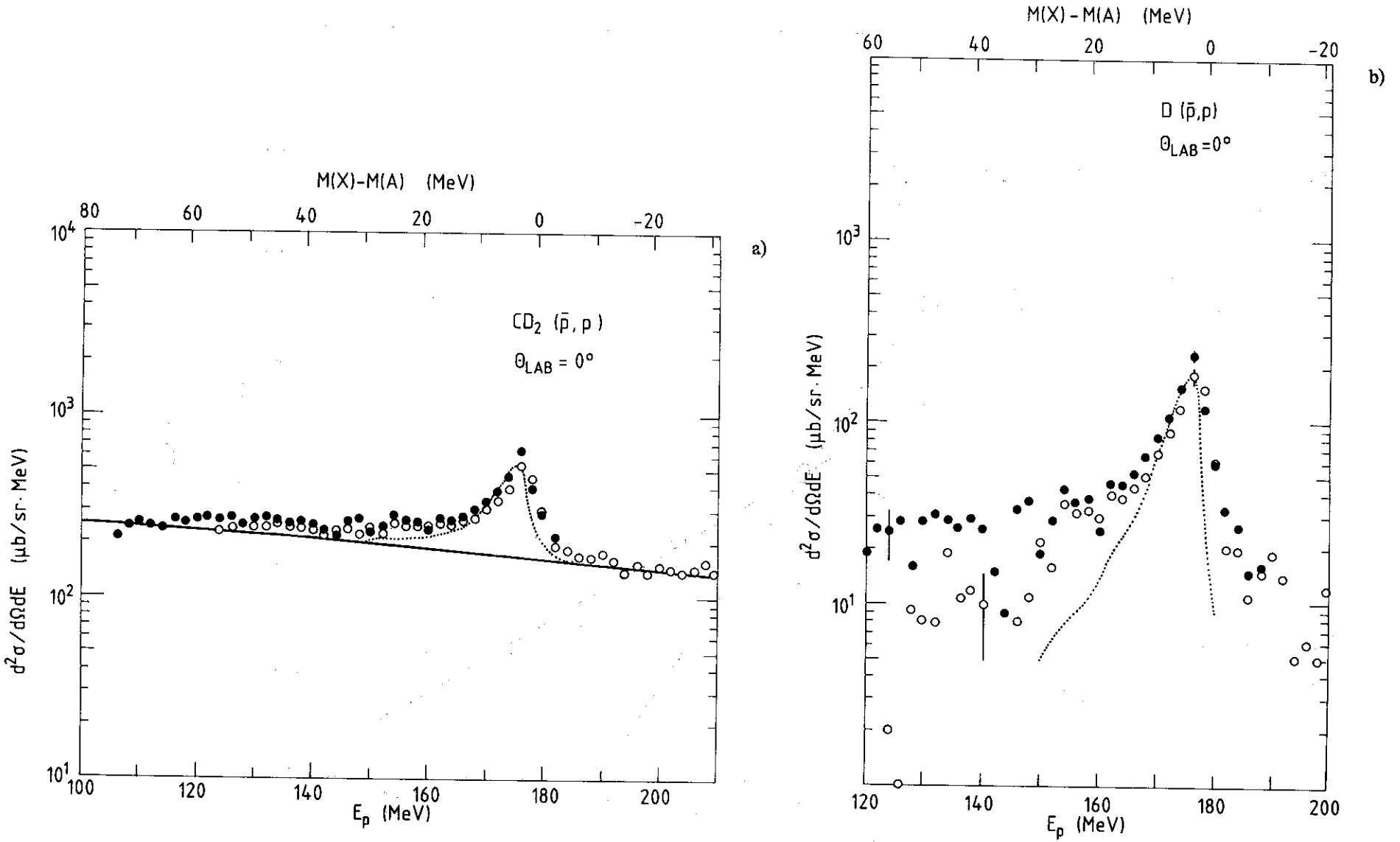
M(X)-M(A) (MeV)
80
60
40
20
0
-20
10^4
10^3
10^2
10^1
CD_2 $(\bar{p}, p)$
$\Theta_{LAB} = 0°$
$d^2\sigma/d\Omega dE$ (μb/sr·MeV)
100
120
140
160
180
200
E_p (MeV)
a)
M(X) - M(A) (MeV)
60
40
20
0
-20
10^3
10^2
10^1
D $(\bar{p},p)$
$\Theta_{LAB} = 0°$
$d^2\sigma/d\Omega dE$ (μb/sr·MeV)
120
140
160
180
200
E_p (MeV)
b)

Fig. 6

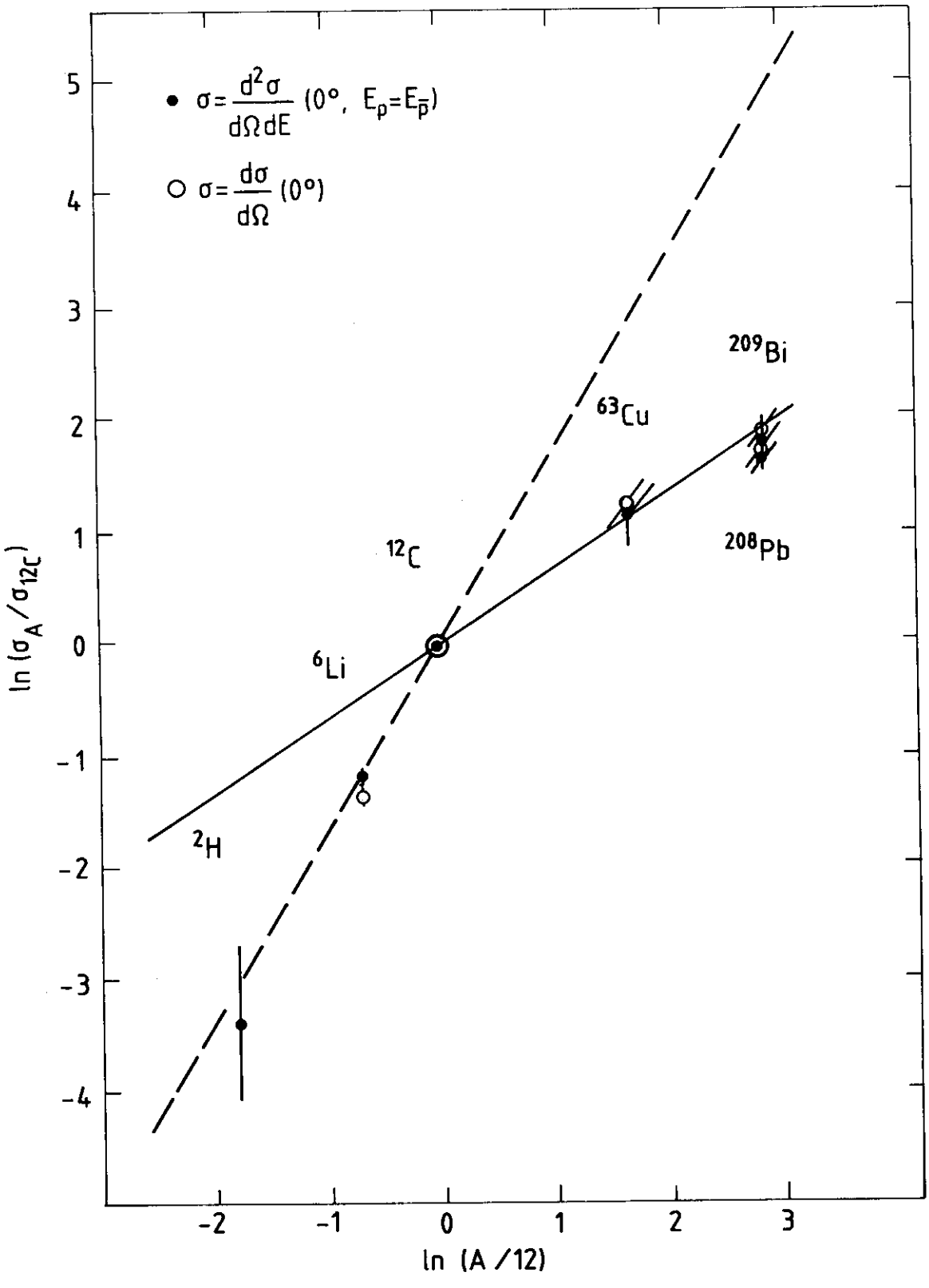
$\sigma = \frac{d^2\sigma}{d\Omega dE}$ (0°, $E_p = E_{\bar{p}}$)
$\sigma = \frac{d\sigma}{d\Omega}$ (0°)
^{209}Bi
^{63}Cu
^{12}C
^{208}Pb
^{6}Li
^{2}H
ln (σ_A / σ_{12C})
ln (A / 12)
5
4
3
2
1
0
-1
-2
-3
-4
-2
-1
0
1
2
3

Fig. 7

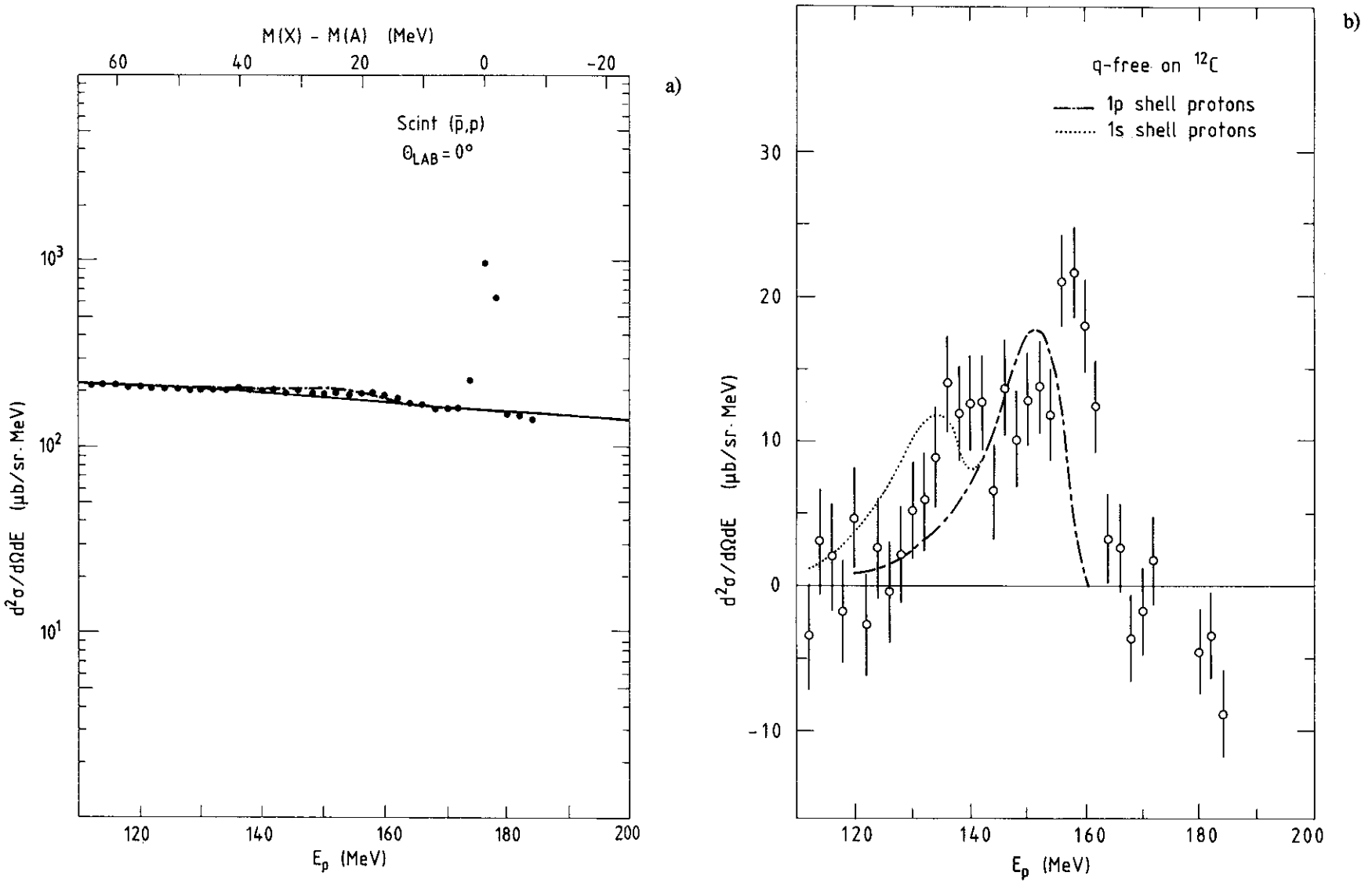
M(X) - M(A) (MeV)
60
40
20
0
-20
Scint (p̄,p)
θLAB = 0°
a)
10³
10²
10¹
d²σ/dΩdE (μb/sr·MeV)
120
140
160
180
200
Ep (MeV)
b)
q-free on ¹²C
1p shell protons
1s shell protons
30
20
10
0
-10
d²σ/dΩdE (μb/sr·MeV)
120
140
160
180
200
Ep (MeV)

Fig. 8